

Muon Pair Production in ep Collisions at HERA

H1 Collaboration

Abstract

Cross sections for the production of two isolated muons up to high di-muon masses are measured in ep collisions at HERA with the H1 detector in a data sample corresponding to an integrated luminosity of 71 pb^{-1} at a centre of mass energy of $\sqrt{s} = 319 \text{ GeV}$. The results are in good agreement with Standard Model predictions, the dominant process being photon-photon interactions. Additional muons or electrons are searched for in events with two high transverse momentum muons using the full data sample corresponding to 114 pb^{-1} , where data at $\sqrt{s} = 301 \text{ GeV}$ and $\sqrt{s} = 319 \text{ GeV}$ are combined. Both the di-lepton sample and the tri-lepton sample agree well with the predictions.

To be submitted to *Phys. Lett. B*

A. Aktas¹⁰, V. Andreev²⁴, T. Anthonis⁴, A. Asmone³¹, A. Babaev²³, S. Backovic³⁵, J. Bähr³⁵,
 P. Baranov²⁴, E. Barrelet²⁸, W. Bartel¹⁰, S. Baumgartner³⁶, J. Becker³⁷, M. Beckingham²¹,
 O. Behnke¹³, O. Behrendt⁷, A. Belousov²⁴, Ch. Berger¹, N. Berger³⁶, T. Berndt¹⁴, J.C. Bizot²⁶,
 J. Böhme¹⁰, M.-O. Boenig⁷, V. Boudry²⁷, J. Bracinik²⁵, W. Braunschweig¹, V. Brisson²⁶,
 H.-B. Bröker², D.P. Brown¹⁰, D. Bruncko¹⁶, F.W. Büsser¹¹, A. Bunyatyan^{12,34},
 G. Buschhorn²⁵, L. Bystritskaya²³, A.J. Campbell¹⁰, S. Caron¹, F. Cassol-Brunner²²,
 K. Cerny³⁰, V. Chekelian²⁵, C. Collard⁴, J.G. Contreras^{7,41}, Y.R. Coppens³, J.A. Coughlan⁵,
 M.-C. Cousinou²², B.E. Cox²¹, G. Cozzika⁹, J. Cvach²⁹, J.B. Dainton¹⁸, W.D. Dau¹⁵,
 K. Daum^{33,39}, B. Delcourt²⁶, N. Delerue²², R. Demirchyan³⁴, A. De Roeck^{10,43}, K. Desch¹¹,
 E.A. De Wolf⁴, C. Diaconu²², J. Dingfelder¹³, V. Dodonov¹², J.D. Dowell³, A. Dubak²⁵,
 C. Duprel², G. Eckerlin¹⁰, V. Efremenko²³, S. Egli³², R. Eichler³², F. Eisele¹³, M. Ellerbrock¹³,
 E. Elsen¹⁰, M. Erdmann^{10,40,e}, W. Erdmann³⁶, P.J.W. Faulkner³, L. Favart⁴, A. Fedotov²³,
 R. Felst¹⁰, J. Ferencei¹⁰, M. Fleischer¹⁰, P. Fleischmann¹⁰, Y.H. Fleming³, G. Flucke¹⁰,
 G. Flügge², A. Fomenko²⁴, I. Foresti³⁷, J. Formánek³⁰, G. Franke¹⁰, G. Frising¹,
 E. Gabathuler¹⁸, K. Gabathuler³², J. Garvey³, J. Gassner³², J. Gayler¹⁰, R. Gerhards¹⁰,
 C. Gerlich¹³, S. Ghazaryan³⁴, L. Goerlich⁶, N. Gogitidze²⁴, S. Gorbounov³⁵, C. Grab³⁶,
 V. Grabski³⁴, H. Grässler², T. Greenshaw¹⁸, M. Gregori¹⁹, G. Grindhammer²⁵, D. Haidt¹⁰,
 L. Hajduk⁶, J. Haller¹³, G. Heinzelmann¹¹, R.C.W. Henderson¹⁷, H. Henschel³⁵, O. Henshaw³,
 R. Heremans⁴, G. Herrera^{7,44}, I. Herynek²⁹, R.-D. Heuer¹¹, M. Hildebrandt³⁷, K.H. Hiller³⁵,
 J. Hladký²⁹, P. Höting², D. Hoffmann²², R. Horisberger³², A. Hovhannisyanyan³⁴, M. Ibbotson²¹,
 M. Ismail²¹, M. Jacquet²⁶, L. Janauschek²⁵, X. Janssen¹⁰, V. Jemanov¹¹, L. Jönsson²⁰,
 C. Johnson³, D.P. Johnson⁴, H. Jung^{20,10}, D. Kant¹⁹, M. Kapichine⁸, M. Karlsson²⁰, J. Katzy¹⁰,
 N. Keller³⁷, J. Kennedy¹⁸, I.R. Kenyon³, C. Kiesling²⁵, M. Klein³⁵, C. Kleinwort¹⁰, T. Kluge¹,
 G. Knies¹⁰, A. Knutsson²⁰, B. Koblitz²⁵, S.D. Kolya²¹, V. Korbel¹⁰, P. Kostka³⁵,
 R. Koutouev¹², A. Kropivnitskaya²³, J. Kroseberg³⁷, J. Kückens¹⁰, T. Kuhr¹⁰, M.P.J. Landon¹⁹,
 W. Lange³⁵, T. Laštovička^{35,30}, P. Laycock¹⁸, A. Lebedev²⁴, B. Leißner¹, R. Lemrani¹⁰,
 V. Lendermann¹⁰, S. Levonian¹⁰, B. List³⁶, E. Lobodzinska^{35,6}, N. Loktionova²⁴,
 R. Lopez-Fernandez¹⁰, V. Lubimov²³, H. Lueders¹¹, S. Lüders³⁶, D. Lüke^{7,10}, T. Lux¹¹,
 L. Lytkin¹², A. Makankine⁸, N. Malden²¹, E. Malinovski²⁴, S. Mangano³⁶, P. Marage⁴,
 J. Marks¹³, R. Marshall²¹, M. Martisikova¹⁰, H.-U. Martyn¹, J. Martyniak⁶, S.J. Maxfield¹⁸,
 D. Meer³⁶, A. Mehta¹⁸, K. Meier¹⁴, A.B. Meyer¹¹, H. Meyer³³, J. Meyer¹⁰, S. Michine²⁴,
 S. Mikocki⁶, I. Milcewicz⁶, D. Milstead¹⁸, F. Moreau²⁷, A. Morozov⁸, I. Morozov⁸,
 J.V. Morris⁵, M. Mozer¹³, K. Müller³⁷, P. Murín^{16,42}, V. Nagovizin²³, B. Naroska¹¹,
 J. Naumann⁷, Th. Naumann³⁵, P.R. Newman³, C. Niebuhr¹⁰, D. Nikitin⁸, G. Nowak⁶,
 M. Nozicka³⁰, B. Olivier¹⁰, J.E. Olsson¹⁰, G. Ossoskov⁸, D. Ozerov²³, C. Pascaud²⁶,
 G.D. Patel¹⁸, M. Peez²², E. Perez⁹, A. Perieanu¹⁰, A. Petrukhin³⁵, D. Pitzl¹⁰, R. Pöschl²⁶,
 B. Portheault²⁶, B. Povh¹², N. Raicevic³⁵, J. Rauschenberger¹¹, P. Reimer²⁹, B. Reisert²⁵,
 C. Risler²⁵, E. Rizvi³, P. Robmann³⁷, R. Roosen⁴, A. Rostovtsev²³, Z. Rurikova²⁵,
 S. Rusakov²⁴, K. Rybicki^{6,†}, D.P.C. Sankey⁵, E. Sauvan²², S. Schätzel¹³, J. Scheins¹⁰,
 F.-P. Schilling¹⁰, P. Schleper¹⁰, S. Schmidt²⁵, S. Schmitt³⁷, M. Schneider²², L. Schoeffel⁹,
 A. Schöning³⁶, V. Schröder¹⁰, H.-C. Schultz-Coulon⁷, C. Schwanenberger¹⁰, K. Sedlák²⁹,
 F. Sefkow¹⁰, I. Sheviakov²⁴, L.N. Shtarkov²⁴, Y. Sirois²⁷, T. Sloan¹⁷, P. Smirnov²⁴,
 Y. Soloviev²⁴, D. South²¹, V. Spaskov⁸, A. Specka²⁷, H. Spitzer¹¹, R. Stamen¹⁰, B. Stella³¹,
 J. Stiewe¹⁴, I. Strauch¹⁰, U. Straumann³⁷, G. Thompson¹⁹, P.D. Thompson³, F. Tomasz¹⁴,
 D. Traynor¹⁹, P. Truöl³⁷, G. Tsipolitis^{10,38}, I. Tsurin³⁵, J. Turnau⁶, E. Tzamariudaki²⁵,
 A. Uraev²³, M. Urban³⁷, A. Usik²⁴, S. Valkár³⁰, A. Valkárová³⁰, C. Vallée²²,

P. Van Mechelen⁴, A. Vargas Trevino⁷, S. Vassiliev⁸, Y. Vazdik²⁴, C. Veelken¹⁸, A. Vest¹, A. Vichnevski⁸, S. Vinokurova¹⁰, V. Volchinski³⁴, K. Wacker⁷, J. Wagner¹⁰, B. Waugh²¹, G. Weber¹¹, R. Weber³⁶, D. Wegener⁷, C. Werner¹³, N. Werner³⁷, M. Wessels¹, B. Wessling¹¹, M. Winde³⁵, G.-G. Winter¹⁰, Ch. Wissing⁷, E.-E. Woehrling³, E. Wunsch¹⁰, W. Yan¹⁰, J. Žáček³⁰, J. Zálešák³⁰, Z. Zhang²⁶, A. Zhokin²³, H. Zohrabyan³⁴, and F. Zomer²⁶

¹ *I. Physikalisches Institut der RWTH, Aachen, Germany^a*

² *III. Physikalisches Institut der RWTH, Aachen, Germany^a*

³ *School of Physics and Space Research, University of Birmingham, Birmingham, UK^b*

⁴ *Inter-University Institute for High Energies ULB-VUB, Brussels; Universiteit Antwerpen (UIA), Antwerpen; Belgium^c*

⁵ *Rutherford Appleton Laboratory, Chilton, Didcot, UK^b*

⁶ *Institute for Nuclear Physics, Cracow, Poland^d*

⁷ *Institut für Physik, Universität Dortmund, Dortmund, Germany^a*

⁸ *Joint Institute for Nuclear Research, Dubna, Russia*

⁹ *CEA, DSM/DAPNIA, CE-Saclay, Gif-sur-Yvette, France*

¹⁰ *DESY, Hamburg, Germany*

¹¹ *Institut für Experimentalphysik, Universität Hamburg, Hamburg, Germany^a*

¹² *Max-Planck-Institut für Kernphysik, Heidelberg, Germany*

¹³ *Physikalisches Institut, Universität Heidelberg, Heidelberg, Germany^a*

¹⁴ *Kirchhoff-Institut für Physik, Universität Heidelberg, Heidelberg, Germany^a*

¹⁵ *Institut für experimentelle und Angewandte Physik, Universität Kiel, Kiel, Germany*

¹⁶ *Institute of Experimental Physics, Slovak Academy of Sciences, Košice, Slovak Republic^{e,f}*

¹⁷ *School of Physics and Chemistry, University of Lancaster, Lancaster, UK^b*

¹⁸ *Department of Physics, University of Liverpool, Liverpool, UK^b*

¹⁹ *Queen Mary and Westfield College, London, UK^b*

²⁰ *Physics Department, University of Lund, Lund, Sweden^g*

²¹ *Physics Department, University of Manchester, Manchester, UK^b*

²² *CPPM, CNRS/IN2P3 - Univ Mediterranee, Marseille - France*

²³ *Institute for Theoretical and Experimental Physics, Moscow, Russia^l*

²⁴ *Lebedev Physical Institute, Moscow, Russia^e*

²⁵ *Max-Planck-Institut für Physik, München, Germany*

²⁶ *LAL, Université de Paris-Sud, IN2P3-CNRS, Orsay, France*

²⁷ *LLR, Ecole Polytechnique, IN2P3-CNRS, Palaiseau, France*

²⁸ *LPNHE, Universités Paris VI and VII, IN2P3-CNRS, Paris, France*

²⁹ *Institute of Physics, Academy of Sciences of the Czech Republic, Praha, Czech Republic^{e,i}*

³⁰ *Faculty of Mathematics and Physics, Charles University, Praha, Czech Republic^{e,i}*

³¹ *Dipartimento di Fisica Università di Roma Tre and INFN Roma 3, Roma, Italy*

³² *Paul Scherrer Institut, Villigen, Switzerland*

³³ *Fachbereich Physik, Bergische Universität Gesamthochschule Wuppertal, Wuppertal, Germany*

³⁴ *Yerevan Physics Institute, Yerevan, Armenia*

³⁵ *DESY, Zeuthen, Germany*

³⁶ *Institut für Teilchenphysik, ETH, Zürich, Switzerland^j*

³⁷ *Physik-Institut der Universität Zürich, Zürich, Switzerland^j*

³⁸ Also at Physics Department, National Technical University, Zografou Campus, GR-15773 Athens, Greece

³⁹ Also at Rechenzentrum, Bergische Universität Gesamthochschule Wuppertal, Germany

⁴⁰ Also at Institut für Experimentelle Kernphysik, Universität Karlsruhe, Karlsruhe, Germany

⁴¹ Also at Dept. Fis. Ap. CINVESTAV, Mérida, Yucatán, México^k

⁴² Also at University of P.J. Šafárik, Košice, Slovak Republic

⁴³ Also at CERN, Geneva, Switzerland

⁴⁴ Also at Dept. Fis. CINVESTAV, México City, México^k

† Deceased

^a Supported by the Bundesministerium für Bildung und Forschung, FRG, under contract numbers 05 H1 1GUA /1, 05 H1 1PAA /1, 05 H1 1PAB /9, 05 H1 1PEA /6, 05 H1 1VHA /7 and 05 H1 1VHB /5

^b Supported by the UK Particle Physics and Astronomy Research Council, and formerly by the UK Science and Engineering Research Council

^c Supported by FNRS-FWO-Vlaanderen, IISN-IIKW and IWT

^d Partially Supported by the Polish State Committee for Scientific Research, SPUB/DESY/P003/DZ 118/2003/2005

^e Supported by the Deutsche Forschungsgemeinschaft

^f Supported by VEGA SR grant no. 2/1169/2001

^g Supported by the Swedish Natural Science Research Council

ⁱ Supported by the Ministry of Education of the Czech Republic under the projects INGO-LA116/2000 and LN00A006, by GAUK grant no 173/2000

^j Supported by the Swiss National Science Foundation

^k Supported by CONACyT

^l Partially Supported by Russian Foundation for Basic Research, grant no. 00-15-96584

1 Introduction

Muon pair production in electron proton scattering proceeds mainly via two-photon interactions, $\gamma\gamma \rightarrow \mu^+\mu^-$, where the incoming photons are radiated from the beam particles [1]. It is important to check the quantitative agreement between experiment and theory in this process, since the understanding of this source of muons is vital in any search for anomalous muon production [2, 3]. The clean experimental signature and the precise Standard Model prediction provide high sensitivity in such searches. In an analysis of multi-electron production [4], six outstanding events, three di-electron and three tri-electron events, were observed with di-electron masses above 100 GeV, a region in which the Standard Model prediction is low. A comparison with di-muon production in the same experiment is therefore particularly interesting.

In this paper, a study of muon pair production in electron¹ proton scattering ($ep \rightarrow e\mu\mu X$) is presented using the H1 detector at the ep collider HERA. The main part of this analysis is based on data with an integrated luminosity of 70.9 pb^{-1} collected with an electron energy of 27.6 GeV and a proton energy $E_p = 920 \text{ GeV}$ ($\sqrt{s} = 319 \text{ GeV}$). These data were recorded in the years 1999 and 2000 in positron proton scattering (60.8 pb^{-1}) and electron proton scattering (10.1 pb^{-1}). Differential cross sections as functions of the invariant mass of the muon pair $M_{\mu\mu}$, the muon transverse momenta P_t^μ and the transverse momentum P_t^X of the hadronic system X are measured for $M_{\mu\mu} > 5 \text{ GeV}$. Results are also given for elastic and inelastic muon pair production separately. In addition, events with high di-lepton masses are studied in $\mu\mu$ and $\mu\mu e$ event samples with cuts adapted to the multi-electron analysis [4]. For this analysis the data at $\sqrt{s} = 301 \text{ GeV}$ ($E_p = 820 \text{ GeV}$) and $\sqrt{s} = 319 \text{ GeV}$ from the years 1994 - 2000 are combined, yielding a total luminosity of 113.7 pb^{-1} .

2 Standard Model Processes

The dominant process for the production of muon pairs in ep interactions is the two-photon reaction illustrated in the Feynman diagram shown in figure 1a. Due to the photon propagators, the momentum transfer to the scattered particles is generally small. While the calculation of the corresponding processes in e^+e^- scattering is rather straightforward, the hadronic structure of the proton must be taken into account in ep scattering. The Feynman diagrams (b)-(e) in figure 1 show additional sources of muon pairs, which are less important than the two-photon reaction (a). They represent the four bremsstrahlung amplitudes in eq scattering with conversion of the radiated photon into a muon pair. The diagrams with the photons radiated from the electron lines can be viewed as Compton scattering of the electron and the photon, which is exchanged with the quark line (QED Compton process). In the phase space considered here, the Cabbibo-Parisi process, diagram (b), dominates (c) due to the pole of the Compton scattering cross section for backward scattered photons in the γe centre of mass system. A similar argument shows that the Drell-Yan process (d) dominates (e). Due to the negative interference of the diagrams (a) and (b) in the low mass region ($M_{\mu\mu} < 10 \text{ GeV}$), the expected cross section in the analysed phase space is about 5 % lower than that calculated when only the contribution of the two-photon process is considered.

¹In this paper “electron” refers to both electron and positron, if not otherwise stated.

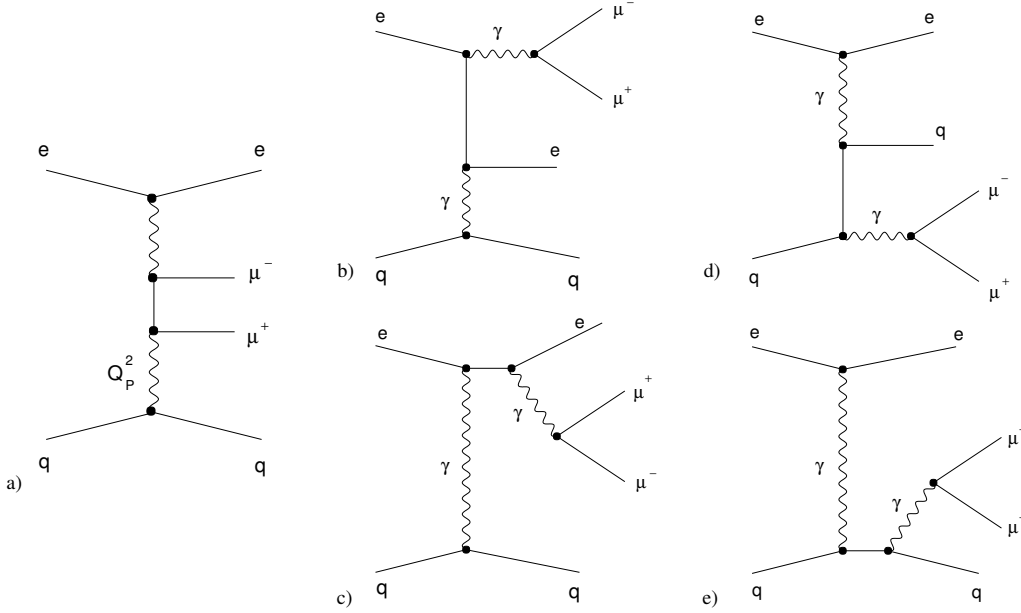


Figure 1: Feynman diagrams for muon pair production in electromagnetic eq interactions, shown for the inelastic case where the scattering takes place from a single quark, such that the proton dissociates to a system X . In the elastic case, the proton scatters coherently. In the general electroweak case, any of the photon propagators can be replaced by a Z boson propagator.

The program GRAPE [5] is used to compute the electroweak theory predictions. It calculates the cross section according to the diagrams (a)-(e) of figure 1 utilising the GRACE [6] program. The program also includes contributions due to Z^0 boson exchange. These contributions become important in cases where the Z^0 radiated from external lines in diagrams (b)-(e) is close to mass shell. The u -pole contribution to the Drell-Yan-process (diagram d) is neglected. Its influence was estimated in [7] and was found to be negligible. Three different approaches are used to describe the proton structure in different phase space regions for the reaction $ep \rightarrow e\mu\mu X$. In the elastic region ($X = p$) the hadronic structure is parametrised by the electromagnetic form factors, which depend on Q_p^2 , the negative four momentum transfer squared between the incoming and outgoing proton. In the quasi-elastic region ($m_p + m_\pi \leq m_X \leq 5 \text{ GeV}$) and the soft inelastic region ($m_X > 5 \text{ GeV}$ and $Q_p^2 < 1 \text{ GeV}^2$), the calculation is based on parametrisations of the proton structure functions, which are given in [8] for the nucleon resonance region ($m_X < 2 \text{ GeV}$) and in [9] above the resonance region. In the deep inelastic region ($m_X > 5 \text{ GeV}$ and $Q_p^2 \geq 1 \text{ GeV}^2$) the cross sections for $eq \rightarrow e\mu\mu q$ are convoluted with the parton density functions of the proton [10]. The GRAPE program is interfaced to PYTHIA [11] and SOPHIA [12] for a complete simulation of the inelastic muon pair production processes. GRAPE allows for QED initial state radiation by adapting the cross section calculation in [13]. Final state radiation is calculated with the parton shower method implemented in PYTHIA.

Vector meson production with subsequent decay into muons is another source of muon pairs in ep scattering. Due to the mass cut ($M_{\mu\mu} > 5 \text{ GeV}$) only the production of Υ mesons needs to be considered. The cross section is calculated using the Monte Carlo generator DIFFVM [14]. Events with two muons also arise from the decay of tau-leptons produced in two-photon col-

lisions $\gamma\gamma \rightarrow \tau\tau$ and from semi-leptonic decays in open heavy quark production ($Q\bar{Q}$, i.e. $c\bar{c}$ and $b\bar{b}$). These reactions are simulated with GRAPE and AROMA [15], respectively. The leading order cross section for b -production calculated with AROMA is normalised to the H1 measurements presented in [16].

3 Data Analysis

3.1 Experimental Conditions

The H1 Detector [17] contains a central tracking detector (full acceptance over the range $25^\circ < \theta < 155^\circ$) and a forward² tracking detector ($7^\circ < \theta < 25^\circ$), which are surrounded by a liquid argon calorimeter ($4^\circ < \theta < 154^\circ$) and a lead-scintillating fibre calorimeter³ (SpaCal calorimeter [18], $153^\circ < \theta < 178^\circ$). The central tracking detector comprises proportional and drift chambers allowing a transverse momentum resolution of $\sigma(P_t)/P_t^2 = 0.005 \text{ GeV}^{-1}$. These detector components are surrounded by a superconducting magnetic coil with a field strength of 1.15 T. The iron return yoke is equipped with streamer tubes forming the central muon detector ($4^\circ < \theta < 171^\circ$). In the forward direction, a proton remnant tagger ($0.06^\circ < \theta < 0.3^\circ$, $z = 24 \text{ m}$) and a forward muon detector ($3^\circ < \theta < 17^\circ$) are used to separate elastic and inelastic processes. The trigger for this analysis is based on single muon signatures from the central muon detector, which are combined with signals from the central tracking detector. In events with large hadronic transverse momenta ($P_t^X > 12 \text{ GeV}$) trigger signals from the liquid argon calorimeter are used in addition.

The procedure to extract cross sections relies on the H1 detector simulation, which is based on the GEANT program [19]. After simulation, the generated events pass through the same reconstruction and analysis chain as the real data. Trigger and muon identification efficiencies are determined with high statistics data samples for the different subdetectors and are incorporated in the simulation. Acceptances and trigger efficiencies for muon pair production are then determined from the Monte Carlo simulation and are used to correct the event yields to obtain cross sections. The overall trigger efficiency for di-muon events is about 70 %. At high hadronic transverse momenta ($P_t^X > 25 \text{ GeV}$) this efficiency is above 98 % [2].

3.2 Event Selection

The event selection and the muon identification are optimised in order to select an event sample consisting of two well identified muons, isolated from other objects in the event. The muon identification [20] is based on measurements from the central tracking detector, the central muon detector and the liquid argon calorimeter. Muon candidates are selected from tracks measured in the central tracking detector, which are linked to tracks measured in the muon detector. Muons which do not reach the muon detector, or enter inefficient regions of the muon detector, can be

²The forward direction and the positive z -axis are given by the proton beam direction. Polar angles θ are defined with respect to the positive z -axis. The pseudorapidity is given by $\eta = -\log(\tan \theta/2)$.

³This device was installed in 1995, replacing a lead-scintillator “sandwich” calorimeter [17].

identified by a central track linked to a signature of a minimal ionising particle in the liquid argon calorimeter. In about 10 % of the selected di-muon events, one of the muons is identified only in the calorimeter. The efficiency for identifying a single muon is typically 75 % in the kinematic range specified below. The momentum and angle measurements are obtained from the central tracking detector.

The analysis requires two muons in the phase space given by:

- polar angle region $20^\circ < \theta_\mu < 160^\circ$;
- transverse momenta $P_t^{\mu_1} > 2 \text{ GeV}$ and $P_t^{\mu_2} > 1.75 \text{ GeV}$;
- invariant mass of the muon pair $M_{\mu\mu} > 5 \text{ GeV}$.

The polar angular range is matched to the acceptance of the central tracking detector, allowing for a precise momentum measurement. The requirement of a minimum transverse momentum ensures good muon identification. The analysis is focused on invariant masses above the J/ψ -mass. Low muon pair masses are studied in [21,22].

Background from cosmic ray muons is suppressed by requiring that:

- the z -coordinate of the event vertex is within 40 cm of the nominal interaction point;
- the opening angle between the two muons is smaller than 165° ;
- the timing of the event determined in the central tracking detector coincides with that of the ep bunch crossing;
- the timing of the two muon track candidates is consistent with their emergence from a common vertex.

The remaining cosmic background contribution is determined to be below 1 %.

An isolation requirement suppresses events with muons from heavy quark decays and events with particles misidentified as muons:

- the distance of the muons to the nearest track or jet⁴ in the pseudorapidity-azimuth plane, $D_{Track,Jet}^\mu = \sqrt{\Delta\eta^2 + \Delta\phi^2}$, is required to be greater than 1. Since at high transverse momenta the background contributions are small, the cut is relaxed to $D_{Track,Jet}^\mu > 0.5$ for $P_t^\mu > 10 \text{ GeV}$.

The remaining contribution of misidentified muons is about 0.5 events, estimated using Monte Carlo simulations of photoproduction and neutral current deep inelastic scattering processes.

The transverse hadronic momentum P_t^X is measured [24] using the liquid argon and SpaCal calorimeters, excluding energy deposits of identified muons or electrons. Electrons are identified in the liquid argon or in the SpaCal calorimeter.

⁴Jets are considered with minimum transverse momentum of $P_t^{Jet} > 5 \text{ GeV}$, identified with the k_t -algorithm [23].

3.3 Systematic Uncertainties

The following uncertainties on the measured cross sections are taken into account.

- The uncertainty on the integrated luminosity measurement is 1.5 %.
- The uncertainty on the trigger efficiency, obtained from an independently triggered event sample, gives a contribution to the systematic uncertainty of 6 %.
- The uncertainty on the identification efficiency of muons is determined by detailed comparison of data and simulation efficiencies for a data sample consisting of events with exactly two tracks and at least one identified muon. This leads to a contribution to the systematic uncertainty of 6 %.
- The uncertainty due to the reconstruction efficiency of the central tracking detector for the two muon tracks contributes with 4 %.
- The uncertainties on the muon θ and ϕ measurements are 3 mrad and 1 mrad, respectively, leading to an effect of up to 1 % on the cross section.
- The systematic uncertainty due to biases in the transverse momentum measurement for high momentum tracks ($P_t > 20$ GeV) is evaluated using the electrons in a neutral current deep inelastic scattering event sample. A scale uncertainty is derived from the ratio of the electron energy measured in the calorimeter to its track momentum measurement. The largest effect on the cross section is 7 % in the highest P_t bin.

These uncertainties added in quadrature lead to a total systematic error of 10 % on the integrated cross section. The uncertainty on the hadronic energy scale (4 % for the liquid argon calorimeter and 7 % for the SpaCal calorimeter) contributes an additional systematic error to the $d\sigma/dP_T^X$ determination.

The uncertainty on the GRAPE calculation is below 1 % for the elastic process [25]. The accuracy of the calculation for the inelastic process is limited by the knowledge of the proton structure. The uncertainty on the structure function parametrisation (quasi-elastic) and the parton density function (deep inelastic) cause an uncertainty smaller than 5 %. The uncertainty on the predictions for other sources of muon pair production is estimated to be 30 % for $Q\bar{Q} \rightarrow \mu\mu$ and 40 % for $\Upsilon \rightarrow \mu\mu$. For the error on the predicted event yields, these theoretical and the experimental uncertainties are added in quadrature with the statistical uncertainty on the Monte Carlo calculation.

4 Results

4.1 Inclusive Two Muon Cross Sections

The cross section for the production of events with at least two muons is measured⁵ and compared with the Standard Model prediction. In total, 1206 data events with two muons are selected, while 1197 ± 124 events are expected according to the Standard Model calculation.

⁵This analysis is based on data taken at a centre of mass energy of $\sqrt{s} = 319$ GeV. More details can be found in [20]. An analysis of data at $\sqrt{s} = 301$ GeV can be found in [26].

No event with more than two muons is observed. In table 1 the contributions of the different Standard Model processes are given, where the errors contain the experimental and model uncertainties. The electroweak muon pair production process dominates all other processes, from which only 28.3 ± 6.7 events are expected. Of the 1206 data events, five events, all with $M_{\mu\mu} < 11$ GeV, have two equally charged muons. This observation is in good agreement with the expectation of 4.1 ± 1.5 events from the decay of heavy quarks.

The cross section, evaluated in the phase space defined by $M_{\mu\mu} > 5$ GeV, $P_t^{\mu_1} > 2$ GeV, $P_t^{\mu_2} > 1.75$ GeV and $20^\circ < \theta_\mu < 160^\circ$, is presented in figure 2a and table 2 as a function of the di-muon mass $M_{\mu\mu}$. The cross section falls steeply over more than four decades over the measured mass range, which extends up to 100 GeV. The shaded histograms show the expected contributions from the Υ and Z^0 resonances, where the latter is also included in the electroweak GRAPE prediction. At small masses minor contributions from open heavy flavour quark production, which are strongly suppressed due to the isolation requirement, and tau-decays are expected. The muon production cross section as a function of the transverse momenta of the two muons is presented in figure 2b and table 3. Both measured cross sections are in good agreement with the Standard Model expectations. The differential cross section as a function of the hadronic transverse momentum P_t^X is also well described, as shown in figure 3 and table 4.

The integrated cross section for electroweak muon pair production, $\sigma_{\mu\mu}^{EW}$, is obtained by subtracting the expected contributions from Υ , $Q\bar{Q}$ and $\tau\tau$ decays. The result is:

$$\sigma_{\mu\mu}^{EW} = (46.4 \pm 1.3 \pm 4.5) \text{ pb.}$$

The first error gives the statistical uncertainty and the second the systematic uncertainty. The measurement is in good agreement with the GRAPE prediction of (46.1 ± 1.4) pb.

4.2 Elastic and Inelastic Muon Pair Production

Elastic ($ep \rightarrow e\mu\mu p$) and inelastic ($ep \rightarrow e\mu\mu X$) muon pair production processes are distinguished by tagging hadronic activity. An event is assigned as inelastic if activity is detected in the proton remnant tagger, the forward muon detector, or in the forward region of the liquid argon calorimeter ($\theta < 10^\circ$) [22]. Events containing tracks in the central or forward tracking detectors not associated to the muons or an identified electron are also considered as inelastic. A total of 631 data events are classified as elastic and 575 as inelastic. This is consistent with the Standard Model expectation, where 611 ± 87 elastic events and 586 ± 96 inelastic events are predicted. The Monte Carlo simulation shows that 92 % of generated inelastic events cause activity in the forward detectors and 93 % of generated elastic events remain untagged. The systematic uncertainty on the separation between elastic and inelastic pair production takes into account the tagging efficiencies of the forward detectors. This leads to an additional uncertainty of 10 % on the elastic and of 12 % on the inelastic cross sections.

Figure 4 and table 5 show the cross sections for elastic and inelastic muon pair production after subtraction of Υ , $Q\bar{Q}$ and $\tau\tau$ contributions. The two spectra are similar and are well described by the electroweak predictions. Elastic muon production contributes somewhat more in the low mass range and inelastic muon production has a slightly harder spectrum. This is

expected, as in elastic processes the electromagnetic form factors of the proton lead to a softer photon spectrum than that produced by radiation from point-like particles (inelastic process).

In the analysed phase space an integrated cross section for elastic di-muon production of

$$\sigma_{\mu\mu}^{el} = (25.3 \pm 1.0 \pm 3.5) \text{ pb}$$

and for inelastic di-muon production of

$$\sigma_{\mu\mu}^{inel} = (20.9 \pm 0.9 \pm 3.2) \text{ pb}$$

are measured. These measurements are in good agreement with the expected cross sections of $(24.6 \pm 0.3) \text{ pb}$ and $(21.5 \pm 1.1) \text{ pb}$, respectively.

4.3 Multi Lepton Events

In addition to the determination of the inclusive di-muon cross section, events with two high P_t muons and possible additional leptons, either muons or electrons, have been studied. In a small fraction of Standard Model electroweak di-muon production processes (figure 1), the electron is scattered through a large angle, such that it is visible in the detector and is not lost in the beam pipe, leading to an observed $e\mu\mu$ final state. Events with three muons in the final state are suppressed within the Standard Model and a tri-muon signal would therefore be of great interest. In order to make use of the highest possible luminosity, data at $\sqrt{s} = 301 \text{ GeV}$ are analysed in addition to the $\sqrt{s} = 319 \text{ GeV}$ sample, resulting in a total luminosity of 113.7 pb^{-1} .

To allow for a comparison with the multi-electron analysis [4], the following cuts are applied for this study:

- two muons in the region $20^\circ < \theta < 150^\circ$;
- transverse momenta $P_t^{\mu 1} > 10 \text{ GeV}$ and $P_t^{\mu 2} > 5 \text{ GeV}$.

Additional muons must be detected in the central region of the detector, $20^\circ < \theta_\mu < 160^\circ$, with a minimum transverse momentum of 1.75 GeV . Additional electrons are searched for in the polar angle range $5^\circ < \theta_e < 175^\circ$ and are required to have a minimum energy of 5 GeV . Such $\mu\mu e$ events are triggered with an efficiency of typically 90 %.

In the examined phase space, 56 di-muon events are found in the data, while 54.7 ± 5.7 events are expected. Among these 56 events, 40 events contain exactly two muons ($\mu\mu$ events), compared with 39.9 ± 4.2 expected. In the other 16 events ($\mu\mu e$ events), one additional electron is observed in the liquid argon or the SpaCal calorimeter, compared with an expectation of 14.9 ± 1.6 events. As expected from the dominant two-photon process, the electron is preferentially found in the backward region of the detector. No event with three or more muons or with two muons and more than one electron is observed.

In figure 5a the di-muon mass distributions of events classified as $\mu\mu$ events or as $\mu\mu e$ events are compared with the theoretical expectations. Both invariant mass distributions are in agreement with the Standard Model calculations. The distribution in M_{12} , the invariant mass of the two leptons with the largest P_t , is shown for the $\mu\mu e$ sample in figure 5b. This mass combination is selected in order to ease comparison with the multi-electron analysis [4], where the scattered electron cannot be identified uniquely. For approximately half of these events, the two leptons with the highest P_t are the electron and a muon. For these events, the mass distribution $M_{12}^{\mu e}$ is also shown in figure 5b. Both mass distributions are compatible with the Standard Model predictions.

For masses $M_{12} > 100$ GeV (> 80 GeV) one $\mu\mu$ event is found, while 0.08 ± 0.01 (0.29 ± 0.03) are expected. This inelastic event with two well identified muons has a mass of $M_{\mu\mu} = 102 \pm 11$ GeV and was recorded at $E_p = 820$ GeV. No event classified as $\mu\mu e$ with $M_{12} > 100$ GeV is observed. The prediction is 0.05 ± 0.01 . These results at high di-lepton masses are in agreement with the Standard Model predictions. In view of the present limited statistics, they cannot be used to draw firm conclusions concerning the high mass excess observed in the multi-electron analysis [4].

5 Conclusion

Isolated muon pair production is analysed for di-muon invariant masses above 5 GeV. The inclusive, elastic and inelastic cross sections are measured. In addition, a $\mu\mu e$ event sample is studied. In all cases, the predictions of the Standard Model are in good agreement with the observations up to the largest di-lepton masses observed.

Acknowledgements

We are grateful to the HERA machine group whose outstanding efforts have made this experiment possible. We thank the engineers and technicians for their work in constructing and maintaining the H1 detector, our funding agencies for financial support, the DESY technical staff for continual assistance and the DESY directorate for support and for the hospitality which they extend to the non DESY members of the collaboration.

References

- [1] J. A. Vermaseren, *Nucl. Phys. B* **229** (1983) 347. 4
- [2] C. Adloff *et al.* [H1 Collaboration], *Eur. Phys. J. C* **5** (1998) 575 [[hep-ex/9806009](#)];
C. Adloff *et al.* [H1 Collaboration], *Phys. Lett. B* **561** (2003) 241 [[hep-ex/0301030](#)]. 4, 6
- [3] J. Agrawal, P. H. Frampton and D. Ng, *Nucl. Phys. B* **386**, 267 (1992) [[hep-ph/9206244](#)];
E. Accomando and S. Petrarca, *Phys. Lett. B* **323** (1994) 212 [[hep-ph/9401242](#)];
E. Accomando, M. Iori and M. Mattioli, [[hep-ph/9505274](#)]. 4

- [4] A. Aktas *et al.* [H1 Collaboration], accepted by Eur. Phys. J. [hep-ex/0307015]. 4, 10, 11
- [5] T. Abe, Comp. Phys. Commun. **136** (2001) 126 [hep-ph/0012029]. 5
- [6] T. Ishikawa *et al.* [MINAMI-TATEYA group Collaboration], “GRACE manual: Automatic Generation of Tree Amplitudes in Standard Models: Version 1.0”, KEK-92-19. 5
- [7] N. Arteaga-Romero, C. Carimalo and P. Kessler, Z. Phys. C **52** (1991) 289. 5
- [8] F. W. Brasse *et al.*, Nucl. Phys. B **110** (1976) 413. 5
- [9] H. Abramowicz and A. Levy, DESY-97-251 [hep-ph/9712415]. 5
- [10] H. L. Lai *et al.* [CTEQ Collaboration], Eur. Phys. J. C **12** (2000) 375 [hep-ph/9903282]. 5
- [11] T. Sjöstrand *et al.*, Comput. Phys. Commun. **135** (2001) 238 [hep-ph/0010017]; T. Sjöstrand, L. Lönnblad and S. Mrenna, [hep-ph/0108264]. 5
- [12] A. Mücke, R. Engel, J. P. Rachen, R. J. Protheroe and T. Stanev, Comp. Phys. Commun. **124** (2000) 290 [astro-ph/9903478]. 5
- [13] J. Fujimoto, M. Igarashi, N. Nakazawa, Y. Shimizu and K. Tobimatsu, Prog. Theor. Phys. Suppl. **100** (1990) 1. 5
- [14] B. List and A. Mastroberardino, “DIFFVM: A Monte Carlo Generator for Diffractive Processes in *ep* Scattering”, Prepared for Workshop on Monte Carlo Generators for HERA Physics, Hamburg, Germany, 27-30 Apr 1998. 5
- [15] G. Ingelman, J. Rathsman and G. A. Schuler, Comp. Phys. Commun. **101** (1997) 135 [hep-ph/9605285]. 6
- [16] C. Adloff *et al.* [H1 Collaboration], Phys. Lett. B **467** (1999) 156 [Erratum-ibid. B **518** (2001) 331] [hep-ex/9909029]. 6
- [17] I. Abt *et al.* [H1 Collaboration], Nucl. Instrum. Meth. A **386** (1997) 310;
I. Abt *et al.* [H1 Collaboration], Nucl. Instrum. Meth. A **36** (1997) 348;
D. Pitzl *et al.*, Nucl. Instrum. Meth. A **454** (2000) 334 [hep-ex/0002044]. 6
- [18] R. D. Appuhn *et al.* [H1 SPACAL Group Collaboration], Nucl. Instrum. Meth. A **386** (1997) 397. 6
- [19] R. Brun *et al.*, “Geant - Detector Description and Simulation Tool”, CERN Program Library Long Writeup W5013, CERN-DD-78-2-REV. 6
- [20] B. Leissner, “Muon Pair Production in Electron-Proton Collisions”, Ph.D. Thesis, RWTH Aachen, DESY-THESIS-2002-049 (available from http://www-h1.desy.de/publications/theses_list.html). 6, 8
- [21] C. Adloff *et al.* [H1 Collaboration], Eur. Phys. J. C **25** (2002) 41 [hep-ex/0205065];
C. Adloff *et al.* [H1 Collaboration], Eur. Phys. J. C **25** (2002) 25 [hep-ex/0205064]. 7

- [22] C. Adloff *et al.* [[H1 Collaboration](#)], Phys. Lett. B **541** (2002) 251 [[hep-ex/0205107](#)]. 7, 9
- [23] S. D. Ellis and D. E. Soper, Phys. Rev. D **48** (1993) 3160 [[hep-ph/9305266](#)]. 7
- [24] C. Adloff *et al.* [[H1 Collaboration](#)], Eur. Phys. J. C **30** (2003) 1 [[hep-ex/0304003](#)]. 7
- [25] T. Abe, private communication. 8
- [26] H.C. Kaestli, “[Muon Pair Production with high Invariant Mass in e+p-Collisions at HERA](#)”, Ph.D. Thesis, ETH Zuerich, ETHZ-IPP I.R.2000-04 (2000) (available from http://www-h1.desy.de/publications/theses_list.html). 8

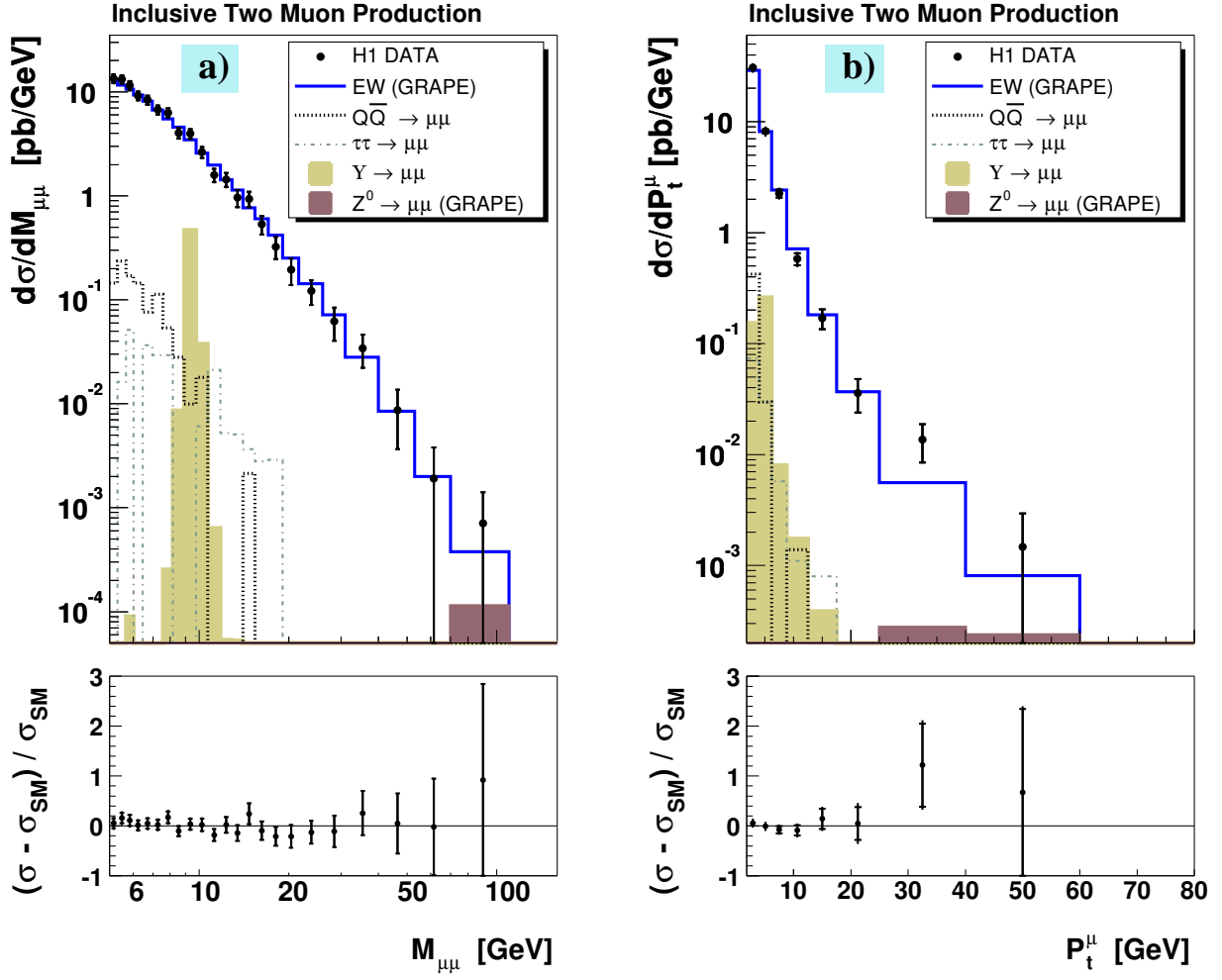


Figure 2: (a) Cross section for the production of two muons in ep interactions as a function of the di-muon mass $M_{\mu\mu}$. (b) Muon production cross section as a function of the muon transverse momenta P_t^μ (two entries per event). The data are compared with Standard Model predictions. See text for the accepted phase space. The relative difference between the data and the sum of all Standard Model contributions is also shown (lower figures). The inner error bars represent the statistical errors, the outer error bars the statistical and systematic errors added in quadrature.

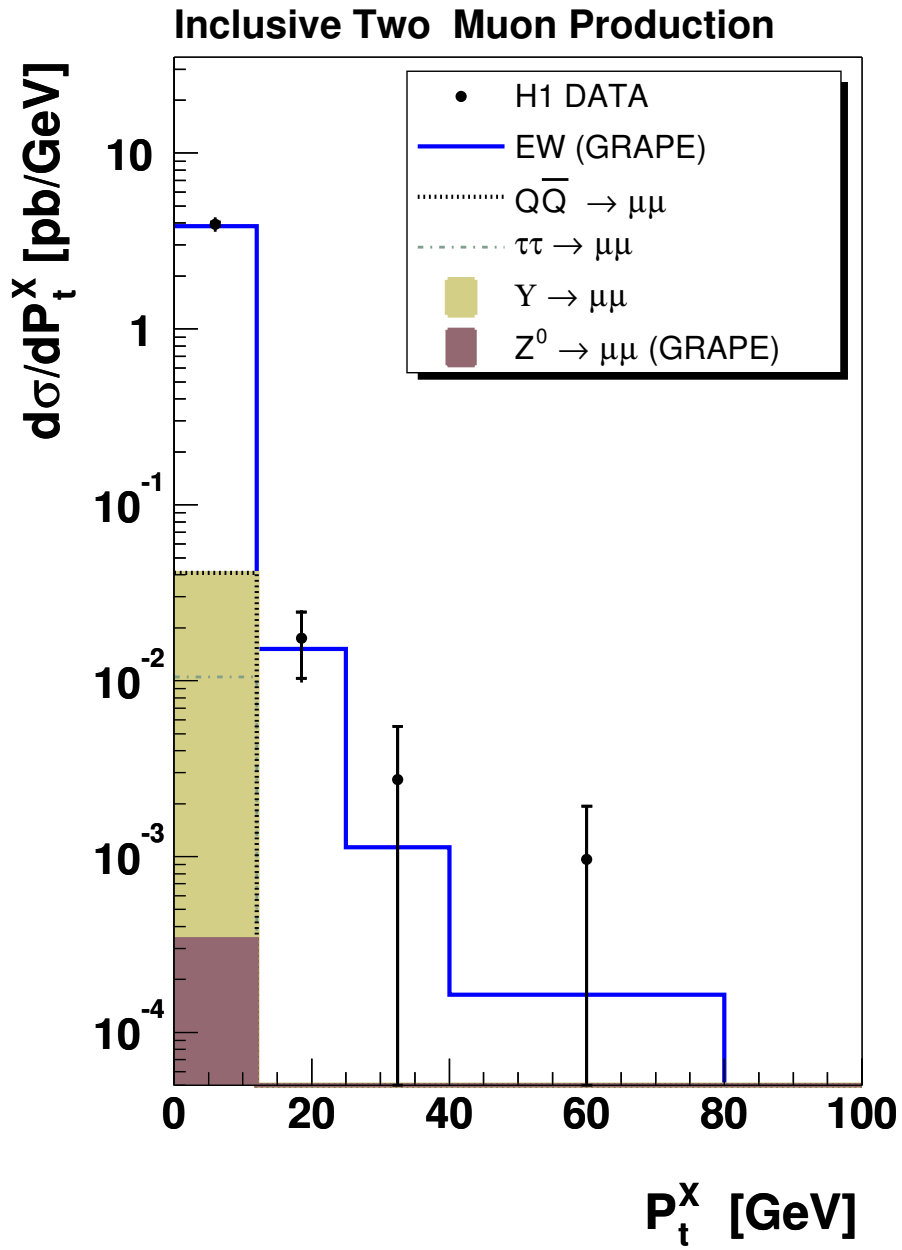


Figure 3: Cross section for two muon production as a function of the hadronic transverse momentum P_t^X . For further details see figure 2.

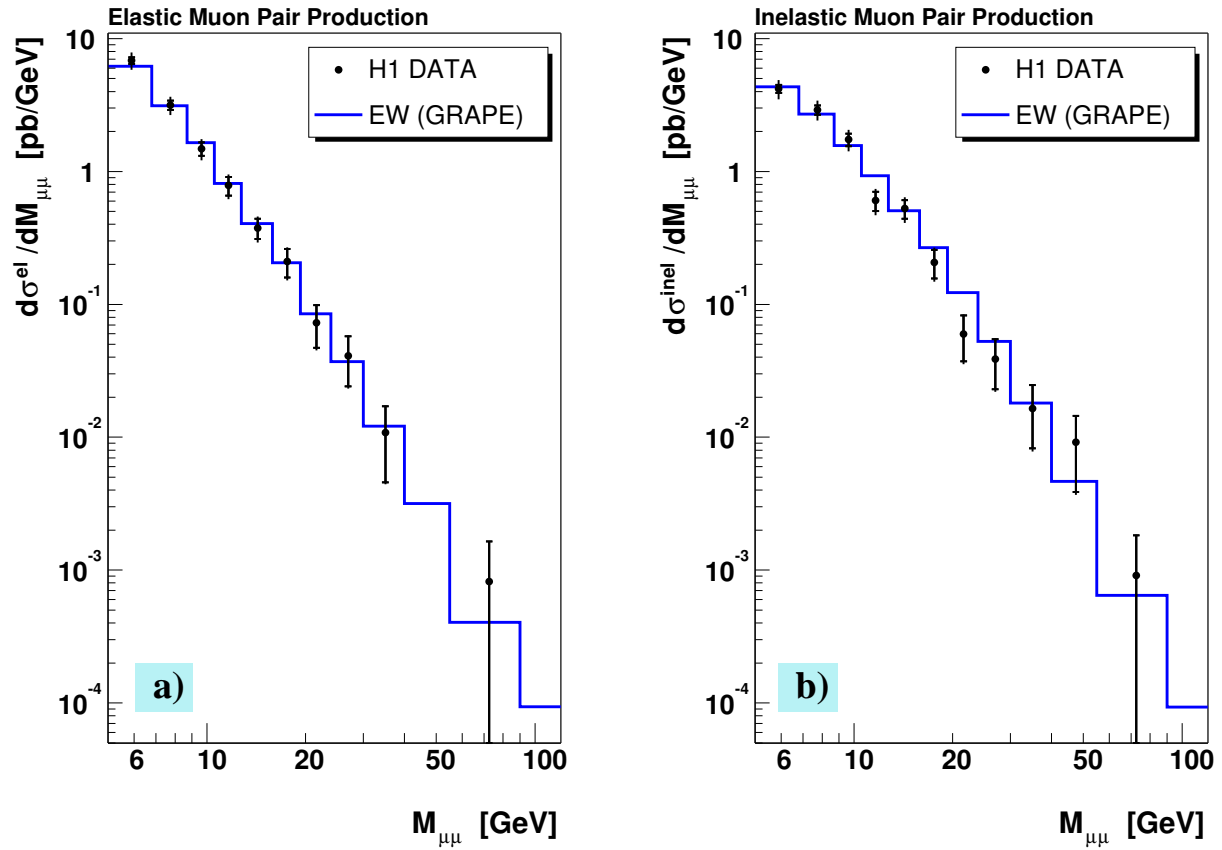


Figure 4: Cross section for electroweak (see text) muon pair production as a function of the invariant mass $M_{\mu\mu}$ for elastically produced muon pairs (a) and for inelastically produced muon pairs (b) compared with the electroweak (EW) prediction using the GRAPE generator. For the accepted phase space see text. The inner error bars represent the statistical errors, the outer error bars the statistical and systematic errors added in quadrature.

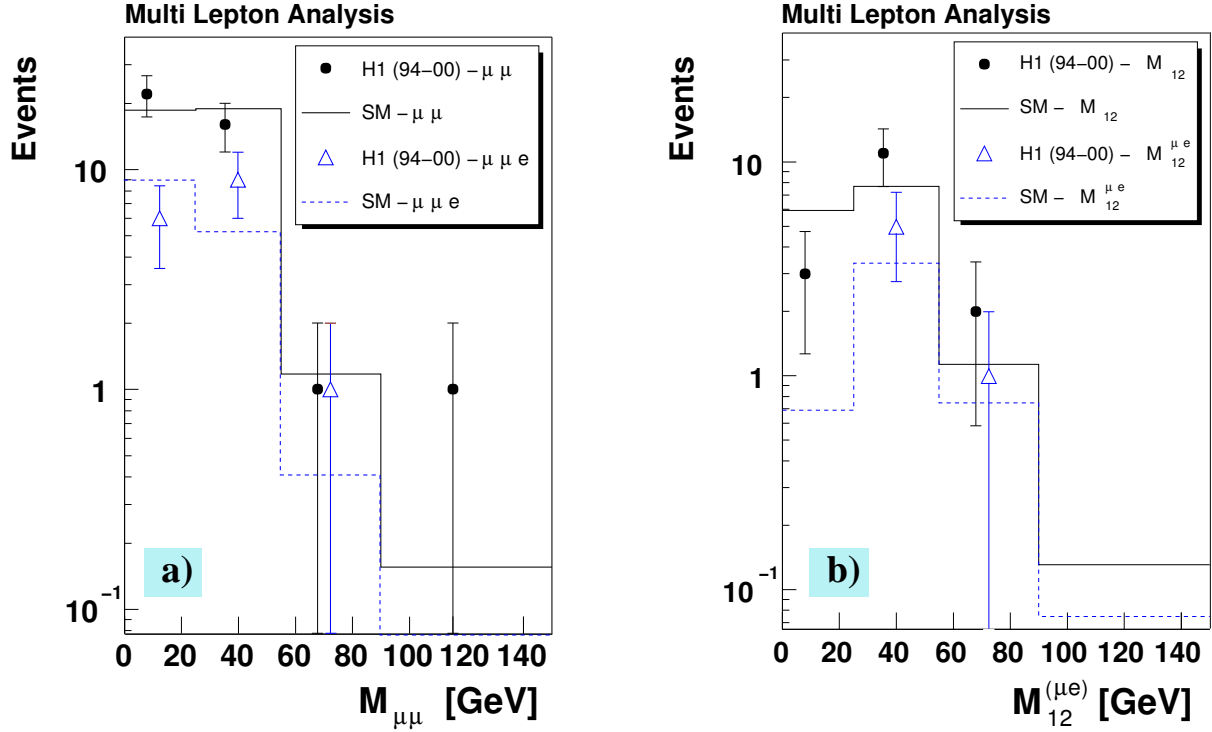


Figure 5: a) Distributions of the invariant mass $M_{\mu\mu}$ for $\mu\mu$ (points) and $\mu\mu e$ (triangles) events, compared with the Standard Model predictions. b) $\mu\mu e$ event distributions of the mass M_{12} of the two highest P_t leptons (points), and of the mass $M_{12}^{\mu e}$ for events where the leptons with the highest P_t are a muon and the electron (triangles). For clarity, the closed data points are shifted slightly to the left. The error bars represent the statistical errors.

Data	SM	EW $\mu^+\mu^-$	$\Upsilon \longrightarrow \mu\mu$	$\tau\tau \longrightarrow \mu\mu$	$Q\bar{Q} \longrightarrow \mu\mu$
1206	1197 ± 124	1169 ± 122	12.3 ± 5.1	4.5 ± 0.6	11.5 ± 3.8

Table 1: The number of selected di-muon events compared with the Standard Model prediction (SM). The dominant electroweak contribution (EW) is determined using the GRAPE generator. The expectations for other contributions are also given.

$M_{\mu\mu}$ range [GeV]	$d\sigma/dM_{\mu\mu}$ [pb/GeV]
5.0 - 5.3	$13.3 \pm 1.3 \pm 1.3$
5.3 - 5.7	$12.8 \pm 1.2 \pm 1.2$
5.7 - 6.0	$12.5 \pm 1.2 \pm 1.2$
6.0 - 6.5	$9.09 \pm 0.89 \pm 0.86$
6.5 - 7.0	$8.85 \pm 0.84 \pm 0.84$
7.0 - 7.6	$7.13 \pm 0.68 \pm 0.68$
7.6 - 8.2	$6.48 \pm 0.63 \pm 0.62$
8.2 - 8.9	$4.11 \pm 0.45 \pm 0.39$
8.9 - 9.8	$4.01 \pm 0.42 \pm 0.38$
9.8 - 10.7	$2.65 \pm 0.33 \pm 0.25$
10.7 - 11.8	$1.54 \pm 0.24 \pm 0.15$
11.8 - 12.9	$1.36 \pm 0.22 \pm 0.13$
12.9 - 14.1	$0.96 \pm 0.19 \pm 0.09$
14.1 - 15.4	$0.88 \pm 0.16 \pm 0.08$
15.4 - 17.1	$0.57 \pm 0.11 \pm 0.05$
17.1 - 19.1	$0.369 \pm 0.089 \pm 0.035$
19.1 - 21.6	$0.165 \pm 0.052 \pm 0.016$
21.6 - 26.0	$0.090 \pm 0.029 \pm 0.009$
26.0 - 31.0	$0.075 \pm 0.025 \pm 0.007$
31.0 - 40.0	$0.027 \pm 0.011 \pm 0.003$
40.0 - 53.0	$0.0093 \pm 0.0054 \pm 0.0009$
53.0 - 70.0	$0.0019 \pm 0.0019 \pm 0.0002$
70.0 - 110.0	$0.00075 \pm 0.00075 \pm 0.00009$

Table 2: Cross section for the production of two muons in ep interactions as a function of the di-muon mass $M_{\mu\mu}$. Di-muon events from Υ , τ -pair and $Q\bar{Q}$ -decays are included in the measurement. The first uncertainty is statistical and the second systematic.

P_T^μ range [GeV]	$d\sigma/dP_T^\mu$ [pb/GeV]
1.8 - 4.0	$30.7 \pm 0.8 \pm 2.9$
4.0 - 6.2	$8.18 \pm 0.37 \pm 0.78$
6.2 - 8.8	$2.26 \pm 0.18 \pm 0.22$
8.8 - 12.5	$0.580 \pm 0.073 \pm 0.055$
12.5 - 17.5	$0.169 \pm 0.034 \pm 0.016$
17.5 - 25.0	$0.036 \pm 0.012 \pm 0.003$
25.0 - 40.0	$0.0136 \pm 0.0052 \pm 0.0014$
40.0 - 60.0	$0.0015 \pm 0.0015 \pm 0.0002$

Table 3: Muon production cross section as a function of the muon transverse momenta P_t^μ (two entries per event). The first uncertainty is statistical and the second systematic.

P_T^X range [GeV]	$d\sigma/dP_T^X$ [pb/GeV]
0.0 - 12.0	$3.94 \pm 0.11 \pm 0.38$
12.0 - 25.0	$0.0174 \pm 0.0071 \pm 0.0029$
25.0 - 40.0	$0.0027 \pm 0.0027 \pm 0.0005$
40.0 - 80.0	$0.00097 \pm 0.00097 \pm 0.00023$

Table 4: Cross section for two muon production as a function of the hadronic transverse momentum P_t^X . The first uncertainty is statistical and the second systematic.

$M_{\mu\mu}$ range [GeV]	$d\sigma^{el}/dM_{\mu\mu}$ [pb/GeV]	$d\sigma^{inel}/dM_{\mu\mu}$ [pb/GeV]
5.0 - 6.8	$6.85 \pm 0.40 \pm 0.95$	$4.19 \pm 0.29 \pm 0.64$
6.8 - 8.7	$3.16 \pm 0.25 \pm 0.44$	$2.91 \pm 0.24 \pm 0.45$
8.7 - 10.6	$1.48 \pm 0.17 \pm 0.21$	$1.74 \pm 0.19 \pm 0.27$
10.6 - 12.8	$0.78 \pm 0.13 \pm 0.11$	$0.60 \pm 0.10 \pm 0.09$
12.8 - 15.9	$0.375 \pm 0.065 \pm 0.052$	$0.525 \pm 0.084 \pm 0.080$
15.9 - 19.3	$0.210 \pm 0.051 \pm 0.029$	$0.207 \pm 0.050 \pm 0.032$
19.3 - 23.9	$0.073 \pm 0.026 \pm 0.010$	$0.060 \pm 0.023 \pm 0.009$
23.9 - 30.0	$0.041 \pm 0.017 \pm 0.006$	$0.039 \pm 0.016 \pm 0.006$
30.0 - 40.0	$0.0108 \pm 0.0063 \pm 0.0015$	$0.0165 \pm 0.0082 \pm 0.0025$
40.0 - 55.0	—	$0.0092 \pm 0.0053 \pm 0.0014$
55.0 - 90.0	$0.00082 \pm 0.00082 \pm 0.00013$	$0.00091 \pm 0.00091 \pm 0.00017$

Table 5: Cross section for electroweak muon pair production as a function of the invariant mass $M_{\mu\mu}$ for elastically produced muon pairs (second column) and inelastically produced muon pairs (third column). Muons from Υ , τ -pair and $Q\bar{Q}$ -decays are considered as background and the expected event yields from these processes are subtracted from the measured event numbers. The first uncertainty is statistical and the second systematic.